Journal of Nuclear Materials 426 (2012) 59–70

Contents lists available at SciVerse ScienceDirect

Journal of Nuclear Materials

journal homepage: www.elsevier.com/locate/jnucmat

SCC growth behaviors of austenitic stainless steels in simulated PWR primary water

T. Terachi [a,*], T. Yamada [b], T. Miyamoto [b], K. Arioka [b]

[a] *Radiological Management Group, The Kansai Electric Power Co. Inc., Japan*
[b] *Institute of Nuclear Safety System, Inc., 64 Sata, Mihama-cho, Mikata-gun, Fukui 919-1205, Japan*

ARTICLE INFO

Article history:
Received 12 July 2011
Accepted 6 March 2012
Available online 16 March 2012

ABSTRACT

The rates of SCC growth were measured under simulated PWR primary water conditions (500 ppm B + 2 ppm Li + 30 cm^3/kg-H_2O-STP DH_2) using cold worked 316SS and 304SS. The direct current potential drop method was applied to measure the crack growth rates for 53 specimens. Dependence of the major engineering factors, such as yield strength, temperature and stress intensity was systematically examined. The rates of crack growth were proportional to the 2.9 power of yield strength, and directly proportional to the apparent yield strength. The estimated apparent activation energy was 84 kJ/mol. No significant differences in the SCC growth rates and behaviors were identified between 316SS and 304SS. Based on the measured results, an empirical equation for crack growth rate was proposed for engineering applications. Although there were deviations, 92.8% of the measured crack growth rates did not exceed twice the value calculated by the empirical equation.

1. Introduction

Stress corrosion cracking (SCC) is an important degradation issue, especially for keeping reliability of pressurized water reactors (PWRs). In nickel-based alloys such as Alloy 600 and their weld metals, SCC has been reported since the 1980s in steam generator tubing, and since the 1990s in the nozzles of pressure vessels and steam generators [1,2]. In comparison with nickel-based alloys, SCC incidence of austenitic stainless steels has not been reported except in some particular cases such as for irradiated materials [3] or in oxygenated environments [4]. However, in recent years, limited examples of SCC were reported in high strain hardened areas or in heat affected zones of stainless steels in PWR primary systems [5,6].

Studies have been done on the SCC behaviors of austenitic stainless steels in simulated environments of light water reactors [7–20]. Cold work (CW) significantly enhanced SCC growth in both BWRs and PWRs. One explanation for the acceleration was reported as due to the reduced plastic zone size at a given stress intensity which produced steeper strain gradients at the crack tip [21–24]. A similar effect of CW on SCC growth was observed in various alloys and environments [24]. Furthermore, formation of vacancies and deformation structures in materials might have some role in the acceleration effect from CW [25]. Arioka et al. [25] reported that the diffusion of vacancies at the grain boundary might be an important process because some similarities were observed between intergranular (IG) creep and SCC in high temperature water. In addition, nickel enrichment was observed ahead of the crack tips at the grain boundary which suggested that grain boundary diffusion did occur before crack advancement. Alternatively, Lozano-Perez et al. [26] pointed out that the length of the localized oxidation region at deformation bands increased with decreasing chromium content in the alloy. Since the deformation bands were formed by CW, the oxidation at crack tips seemed to have some role in the SCC growth process.

Rolling direction of CW also affected the crack growth rate (CGR). Using 316 stainless steel (316SS), Arioka et al. [27] found that much faster CGRs were observed in the *T–L* orientation than in the *T–S* orientation; a schematic drawing showing definitions of the orientations is given in Fig. 1. Moshier and Brown [20] reported that CGRs were 10 times more rapid in the *S–T* orientation compared to the *L–T* orientation of Alloy 600. The effect of the CW orientation is not well clarified, except that *S–L*, *S–T* and *T–L* orientations provide aggressive cracking compare to *T–S* and *L–S* orientations [20,27,28]. In considering an actual component with elbow structures, for example, while the bending method is not simple rolling, the crack direction for penetration might correspond to *T–S* or *L–S* orientations. In the present paper, *T–S* orientation specimens were used to estimate CGRs for 316SS and 304SS specimens.

Elucidating the temperature dependence on SCC is of great importance not only for a mechanistic viewpoint, but also for the prediction of CGRs of each system at operating power plants. The reported activation energies of SCC in CW stainless steels under PWR conditions range from 56 kJ/mol to 107 kJ/mol [25,29,30]. Several factors including chemical reaction, diffusion at a grain boundary and mechanical properties have some potential to change the apparent activation energy of cracking [31]. If the

* Corresponding author. Tel.: +81 770 32 3650.
E-mail address: terachi.takumi@a4.kepco.co.jp (T. Terachi).

0022-3115/$ - see front matter © 2012 Elsevier B.V. All rights reserved.
http://dx.doi.org/10.1016/j.jnucmat.2012.03.013

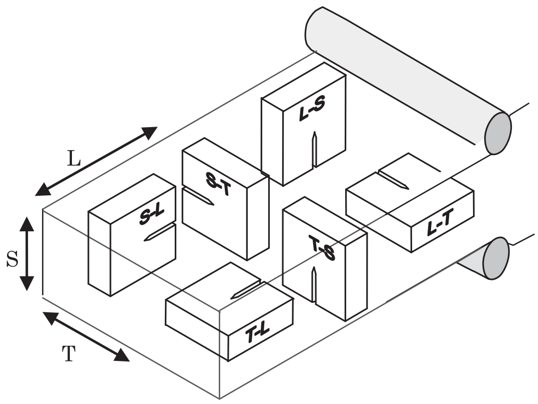

Fig. 1. Schematic of rolling orientation in relation to the longitudinal (L), thickness (T) and short transverse (S) directions.

surface reaction at a metal–water interface controls the thermal activation process, activation energy will be affected by the water chemistry conditions. From this perspective, obtaining systematic CGRs is important to get accurate activation energies and elucidate the SCC mechanism.

The objective of this study is to quantify systematically the rate of SCC growth of CW 316SS and 304SS in PWR primary water conditions. The influences of yield strength, temperature dependence and stress intensity factors were examined using 53 0.5T compact tension (CT) specimens.

2. Experimental

2.1. Materials

Specimens of 316SS and 304SS were used to determine the CGRs of SCC in hydrogenated high temperature water. The elemental components and material properties are listed in Tables 1 and 2, respectively. The materials were solution-treated at 1060–1080 °C for 10 min then water quenched. To examine the influence of CW, materials were cold-rolled in one dimension to produce 5%, 10%, 15% and 20% reductions in thickness at room temperature (RT).

The yield strengths of specimens at the test temperature were required to confirm the validity of the SCC test, and they were estimated from the measured data at RT and 320 °C using the trend of reported temperature dependence as shown in Fig. 2 [32]. The estimated values are listed in Table 3.

2.2. Specimen preparation

Specimen morphology was as shown in Fig. 3. The CT specimens were extracted from the CW plate. Prior to the CGR measurement, each specimen was pre-cracked in air by fatigue stress by applying a symmetrical triangle wave equal to or less than 10 Hz. The stress intensity factor of pre-cracking was controlled so that it did not exceed 80% of the stress intensity factor of the initial CGR measurement. However due to the difficulty of pre-cracking under quite a small stress condition, the minimum stress intensity factor for pre-cracking was fixed to 10 MPa$\sqrt{m}$. Target length of a pre-crack was set to 2–2.5 mm and actual length was assessed after the SCC test.

2.3. Crack growth rate measurements

All CGR measurements were carried out using water circulation type autoclaves. An example of the SCC test facility set-up is shown in Fig. 4. Specimens were immersed in simulated PWR primary water that contained 500 ppm boron as boric acid, 2 ppm lithium as LiOH and 30 cm^3-STP/kg-H_2O of dissolved hydrogen (DH). Dissolved oxygen in the water was continuously monitored at the inlet of the autoclave and controlled not to exceed 5 ppb. CGR trends of most specimens were monitored by the direct current potential drop method (PDM) described in ASTM standard E647-11[33]. Applied reversing direct current was 0.8–5 A and potential drop signals were detected by a high precision nano-voltmeter. Electric noise was reduced by analog and digital filtering, and noise possibly derived from temperature fluctuation of the water (less than ±1 °C) was eliminated by a smoothing technique. Calculated CGR resolution from PDM signal was roughly 10–50 μm. RT which would also affect the entire monitoring system was maintained 25 ± 2 °C.

Example CGR measurement results are shown in Fig. 5. A trapezoidal wave loading with $R = 0.7$, $\omega = 0.017\ s^{-1}$ was applied every 4 h for 10–20 days to initiate crack growth through a grain

Table 2
Mechanical properties of alloys.

Cold work (%)	Yield strength (N/mm^2) (320 °C)	Tensile strength (N/mm^2) (320 °C)	Elongation (%) (320 °C)	HV (1 kg)
316SS				
5	243	458	36	184
10	345	495	29	219
15	495	565	15	254
20	572	607	10	270
304SS				
5	270	434	38	205
10	365	466	32	214
15	436	503	24	243
20	498	564	16	267

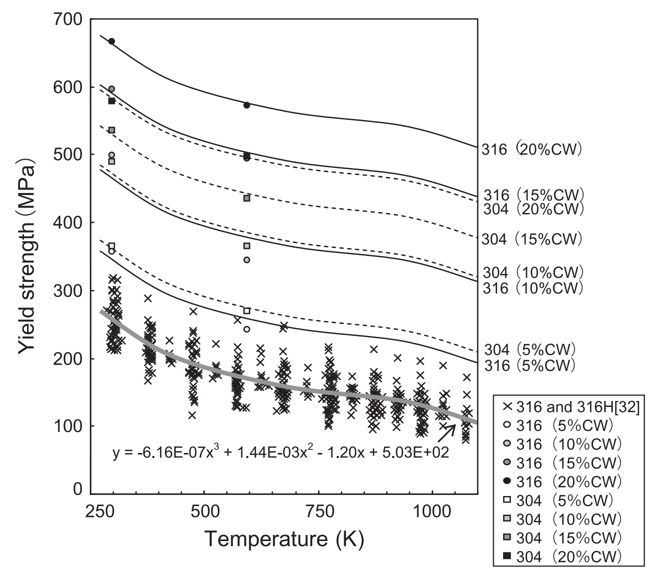

Fig. 2. Yield strength as a function of temperature [32]. Prediction curves for CW alloys are roughly parallel to the reference data.

Table 1
Compositions of alloys (mass%).

	C	Si	Mn	P	S	Ni	Cr	Mo
316SS	0.047	0.45	1.42	0.024	0.001	11	16.45	2.07
304SS	0.04	0.31	1.59	0.031	0.001	9.21	18.34	0.37

Heat treatment: 316SS, 1080 °C; 304SS, 1060 °C, water quenched.

Table 3
Estimated yield strength at high temperature (N/mm^2).

Temperature (°C)	316SS				304SS			
	5%CW	10%CW	15%CW	20%CW	5%CW	10%CW	15%CW	20%CW
250	268	389	513	587	285	395	453	506
270	264	385	509	583	281	391	449	502
280	262	383	507	581	279	389	447	500
290	260	382	506	580	278	388	446	499
300	259	380	504	578	276	386	444	497
310	257	379	502	576	275	385	443	496
320	256	377	501	575	273	383	441	494
330	254	376	500	574	272	382	440	493
340	253	374	498	572	270	380	438	491
350	252	373	497	571	269	379	437	490
360	251	372	496	570	268	378	436	489

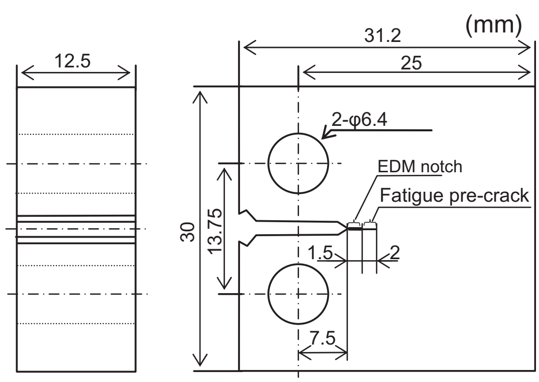

Fig. 3. Example of compact tension specimen morphology.

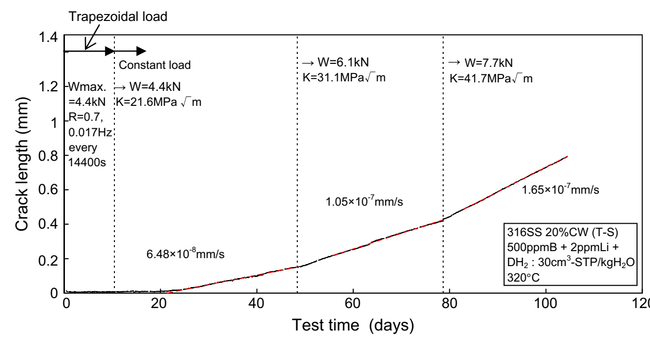

Fig. 5. Potential drop measurement of 316SS (20%CW, *T–S*, Specimen No. S6C2F) under simulated PWR primary water conditions.

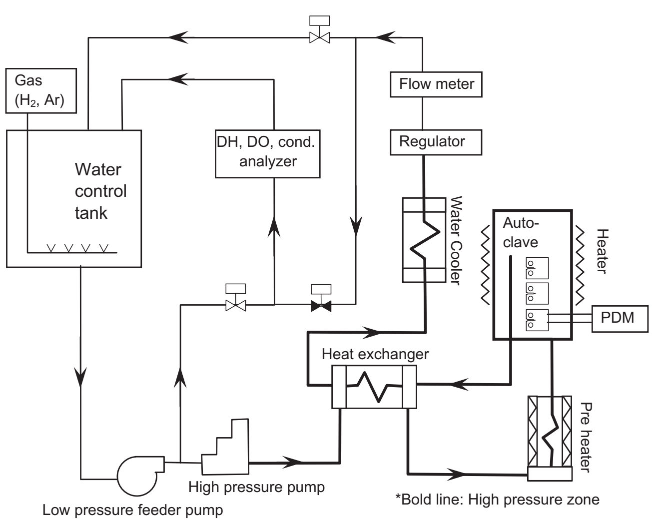

Fig. 4. Example of SCC test equipment set-up.

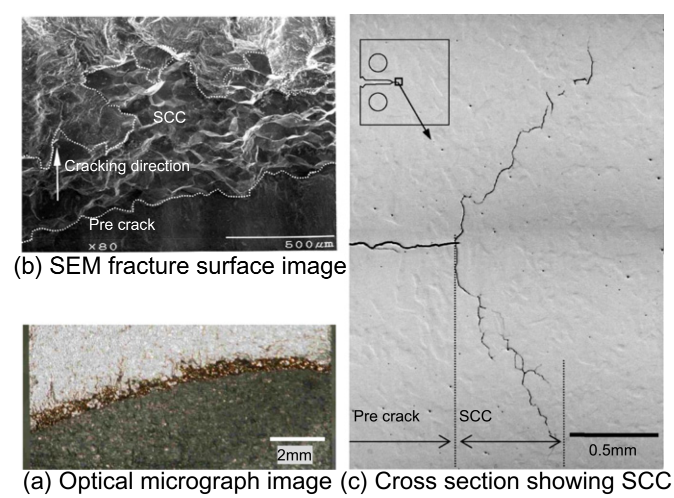

Fig. 6. Example of fracture surface and cross-sectional observation of 316SS (20%CW, *T–S*, Specimen No: S6C2F), tested under simulated PWR primary water conditions (500 ppm B + 2 ppm Li + DH_2: 30 cm^3-STP/kg H_2O, 320 °C).

boundary. After the trapezoidal wave loading, the stress condition was kept constant to measure the CGR data. Several CGR data were obtained from a specimen by changing the test conditions such as applied stress, as shown in Fig. 5, or the temperature condition. After the test, the specimens were fractured by fatigue stress in air, and the crack length was measured using a scanning electron microscope (SEM). The PDM signals for the CGR were corrected by means of the average crack length that was measured by SEM fracture surface observation. However, on account of the difficulty for maintaining electrical insulation in high temperature water, the PDM technique was not applied for tests above 330 °C. This is because the present system used polytetrafluoroethylene for insulation. In the case of no PDM signal, trapezoidal wave loading was not applied as a starter due as it was not possible to eliminate the effect of fatigue loading.

3. Results

3.1. Crack growth rate measurements

Fig. 6 shows an example of a fracture surface and a cross-sectional observation of a tested 316SS (20%CW) specimen

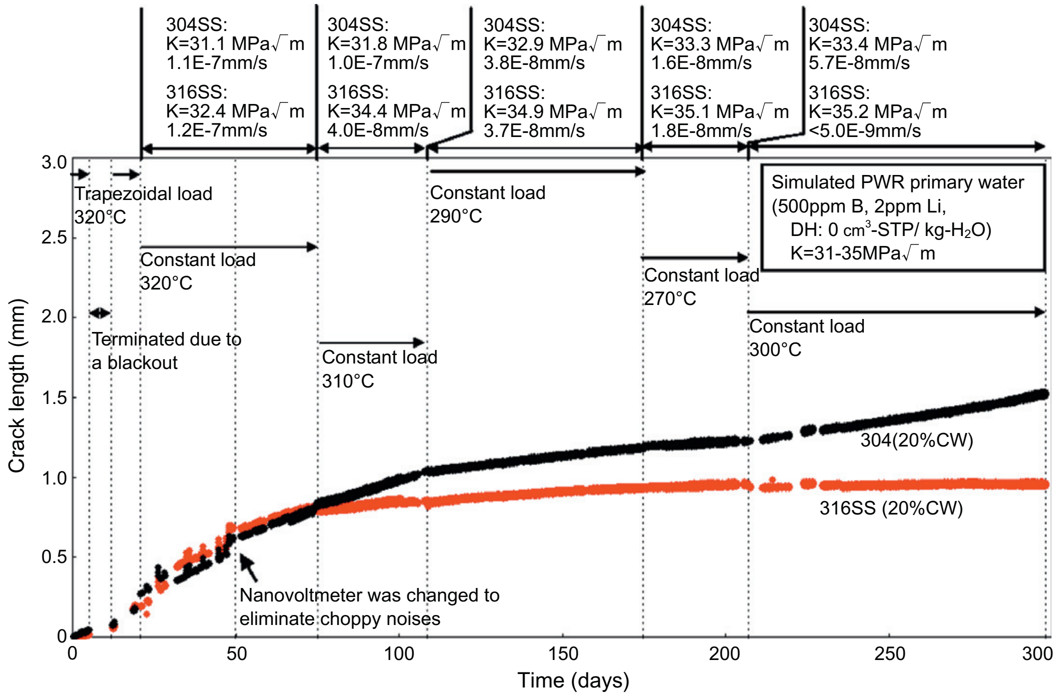

Fig. 7. Crack growth rate measurement of 316SS (20%CW, *T–S*, Specimen No. G316A8) and 304SS (20%CW, *T–S*, Specimen No. G304E-9) under simulated PWR primary water conditions.

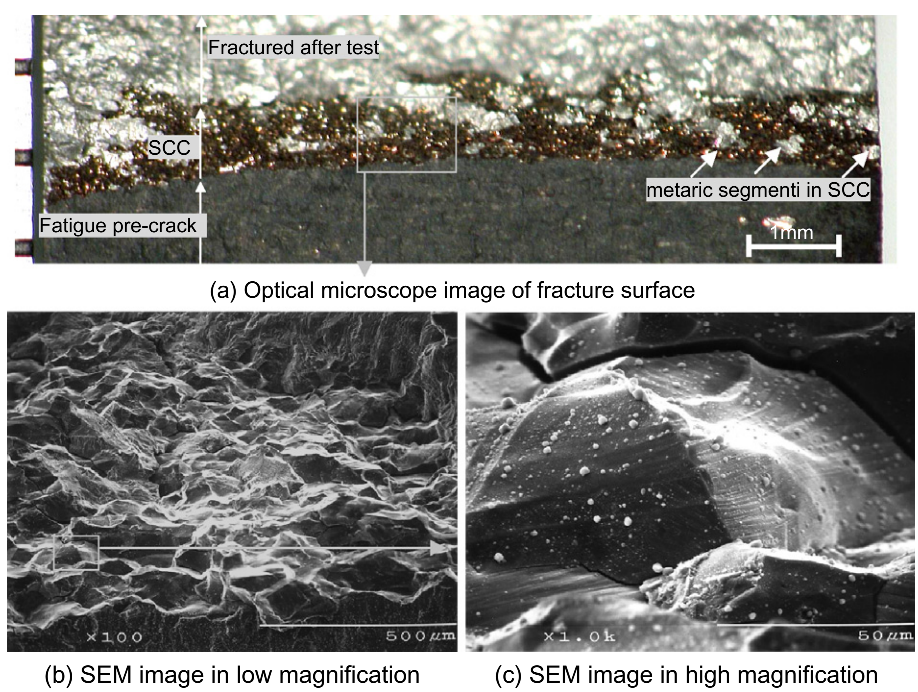

Fig. 8. Fracture surface of 316SS (20%CW, *T–S*, Specimen No. G316A8), tested under simulated PWR primary water conditions for 6650 h (500 ppm B + 2 ppm Li + DH_2: 30 cm^3-STP/kg H_2O, 270–320 °C).

revealing that the SCC propagated through the grain boundary. The cross-sectional image showed the crack deviated in two directions, approximately 60° from normal cracking. This kind of splitting was reported on *T–S* orientation CW specimens [27]. Even though the mechanism is not clear, the important crack orientation for operating plants is propagation in the wall thickness direction; therefore in the paper, the crack length was defined as the measured length observed from the loading direction using an SEM image. Theoretically branching also affects the calculation of stress intensity factor, because the stress to open the crack mouth decreases and shear stress increases [34]. However it is difficult to determine the branched angle for the entire thickness especially in specimens with short cracks, so from a practical viewpoint, apparent stress intensity factor was calculated using the ASTM E399-09 [35] code

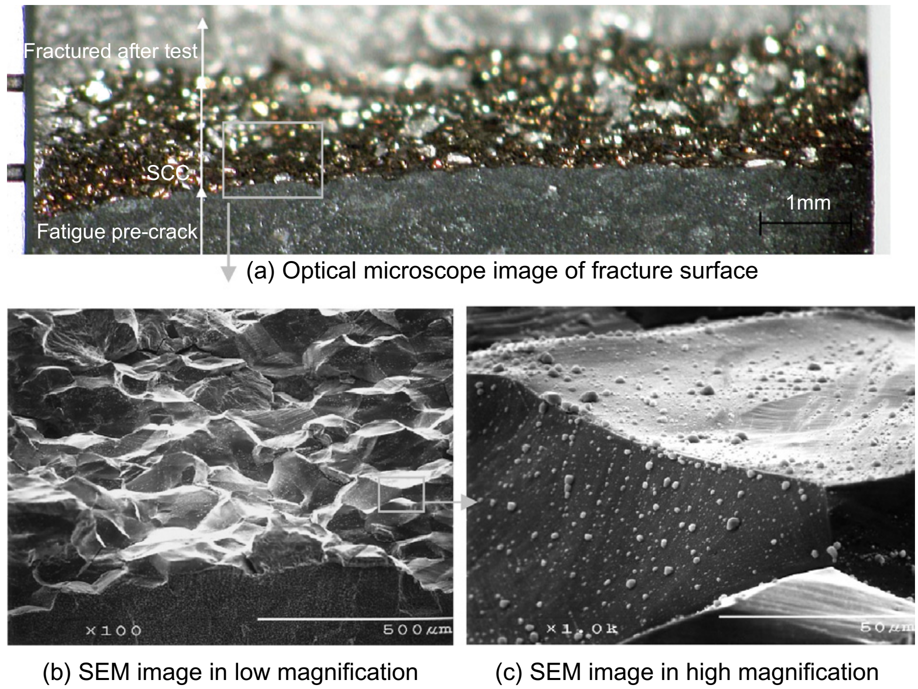

Fig. 9. Fracture surface of 304SS (20%CW, *T–S*, Specimen No. G304E-9), tested under simulated PWR primary water conditions for 6650 h (500 ppm B + 2 ppm Li + DH_2: 30 cm^3-STP/kg H_2O, 270–320 °C).

Table 4
SCC growth rates of 316SS (5–10%CW, *T–S*).

Specimen no.	Cold work (%)	Temperature (°C)	Test time (days)	Apparent stress intensity factor (MPa$\sqrt{m}$)	Average crack length increment (mm)	Average crack growth rate (mm/s)
S6C5A	5	290	31	34.1	0.02	6.3E-09
	5	300	55	34.0	0.02	4.2E-09
	5	320	42	26.1	0.02	5.5E-09
	5	320	36	33.9	0.05	1.5E-08
GC S6C5 C	5	320	182	31.9	0.27	1.7E-08
S6C10A	10	320	26	20.3	<0.01	<5.0E-09
	10	320	32	27.9	0.05	1.8E-08
	10	320	28	34.6	0.11	4.4E-08
S6C10B	10	290	60	30.2	<0.01	<5.0E-09
	10	270	35	30.2	<0.01	<5.0E-09
	10	310	25	30.2	0.02	9.6E-09
S6C10D	10	300	71	30.9	0.04	5.8E-09
S6C10C	10	290	71	30.0	<0.01	<5.0E-09
S6C10E	10	290	27	26.1	0.01	<5.0E-09
	10	290	15	40.2	0.03	2.3E-08
	10	320	47	25.8	0.15	3.6E-08
S6C10-2	10	320	55	28.0	<0.01	<5.0E-09
	10	310	33	22.9	<0.01	<5.0E-09
	10	290	49	28.0	<0.01	<5.0E-09
	10	270	17	28.0	<0.01	<5.0E-09
	10	300	98	28.0	<0.01	<5.0E-09
GS6C10-4	10	320	41	28.2	0.166	4.7E-08
G316-10-TS-1	10	360	20	30.9	<0.01	<5.0E-09
G316-10-TS-2	10	340	34	31.7	<0.01	<5.0E-09
G316-10-TS-3	10	330	61	31.7	0.07	1.3E-08

for non-branched cracks. The apparent stress intensity factors in this paper were the averaged values during crack propagation.

Crack propagation curves of 316SS (20%CW) and 304SS (20%CW) below 320 °C are shown in Fig. 7. Initially a trapezoidal wave load was applied for IG cracking, and then it was switched to a constant load for a SCC test. The crack growth rates of 316SS (20%CW) and 304 (20%CW) at 320 °C were estimated from the PDM trend as 1.2×10^{-7} mm/s and 1.1×10^{-7} mm/s, respectively. While similar CGRs were obtained at 320 °C, slower CGRs in 316SS (20%CW) were observed at 310 °C. During the test at 290 °C and 270 °C, similar CGRs trend were observed in both steel types, and they decreased with decreasing temperature conditions. When

Table 5
SCC growth rates of 316SS (15%CW, *T–S*).

Specimen no.	Cold work (%)	Temperature (°C)	Test time (days)	Apparent stress intensity factor (MPa$\sqrt{m}$)	Average crack length increment (mm)	Average crack growth rate (mm/s)
S6C15A	15	320	26	20.8	0.10	4.4E-08
	15	320	32	29.1	0.19	6.9E-08
	15	320	28	36.9	0.28	1.2E-07
S6C15B	15	270	35	30.8	0.02	6.1E-09
	15	290	60	30.7	0.07	1.3E-08
	15	310	25	30.4	0.04	1.7E-08
S6C15C	15	290	71	30.0	0.01	<5.0E-09
S6C15D	15	300	71	30.1	0.21	3.4E-08
S6C15E	15	290	15	25.7	0.02	1.4E-08
	15	290	27	25.7	0.04	1.6E-08
	15	290	15	39.7	0.07	5.0E-08
	15	320	47	25.3	0.18	4.5E-08
S6C15-4	15	320	27	8.5	<0.01	<5.0E-09
	15	290	84	13.0	0.04	5.6E-09
	15	320	84	13.0	0.03	4.1E-09
S6C15-5	15	290	56	13.5	0.10	2.0E-08
	15	290	21	17.3	0.04	2.2E-08
	15	290	63	17.9	0.01	<5.0E-09
	15	290	48	21.8	0.01	<5.0E-09
	15	290	50	21.9	0.09	2.0E-08
	15	290	35	26.1	<0.01	<5.0E-09
G316 15-TS-1	15	360	30	31.7	<0.01	<5.0E-09
G316-15-TS-2	15	340	34	31.6	<0.01	<5.0E-09
G316-15-TS-5	15	330	61	30.9	0.11	2.1E-08
G316-15-TS-3	15	250	409	30.1	0.08	2.3E-09

Table 6
SCC growth rates of 316SS (20%CW, *T–S*).

Specimen no.	Cold work (%)	Temperature (°C)	Test time (days)	Apparent stress intensity factor (MPa$\sqrt{m}$)	Average crack length increment (mm)	Average crack growth rate (mm/s)
S6C2E	20	250	75	38.4	<0.01	<5.0E-09
	20	270	32	40.8	0.05	1.7E-08
S6C20D	20	290	27	26.6	0.12	5.0E-08
	20	290	15	26.9	0.09	7.1E-08
	20	290	15	42.2	0.24	1.8E-07
	20	300	71	30.1	0.83	1.4E-07
	20	320	47	25.8	0.39	9.5E-08
S6C2E	20	290	30	38.6	0.10	3.8E-08
	20	290	22	40.2	0.07	3.4E-08
	20	320	17	39.3	0.20	1.4E-07
S6C2D	20	320	61	29.6	0.55	1.1E-07
S6C2F	20	320	30	21.6	0.17	6.5E-08
	20	320	38	31.1	0.35	1.1E-07
	20	320	26	41.7	0.37	1.7E-07
G316A8	20	320	55	32.4	0.57	1.2E-07
	20	310	33	34.4	0.11	4.0E-08
	20	290	66	34.9	0.21	3.7E-08
	20	270	32	35.1	0.05	1.8E-08
	20	300	91	35.2	<0.01	<5.0E-09
S6C20-1	20	290	83	13.6	0.04	5.6E-09
	20	320	84	13.5	<0.01	<5.0E-09
S6C20-2	20	290	56	14.4	0.09	1.9E-08
	20	290	63	19.3	0.21	3.8E-08
	20	290	21	20.6	0.03	1.5E-08
	20	290	48	24.0	0.21	5.1E-08
	20	290	50	25.7	0.29	6.8E-08
	20	290	35	29.7	0.28	9.1E-08
GCS6C20-K	20	360	30	32.5	0.52	2.0E-07
GCS6C020-L	20	340	34	32.9	0.79	2.7E-07
GCS6C20-M	20	340	30	32.9	0.88	3.4E-07
GCS6C20-N	20	350	30	32.9	0.86	3.3E-07
GCS6C20-O	20	360	30	32.1	0.36	1.4E-07
G316-20-TS-1	20	250	409	31.7	0.28	7.9E-09

Table 7
SCC growth rates of 304SS (5–15%CW, *T–S*).

Specimen no.	Cold work (%)	Temperature (°C)	Test time (days)	Apparent stress intensity factor (MPa$\sqrt{m}$)	Average crack length increment (mm)	Average crack growth rate (mm/s)
G304B-1	5	290	72	20.8	<0.01	<5.0E-09
	5	290	58	25.8	<0.01	<5.0E-09
	5	290	58	31.2	0.16	3.3E-08
G304B-2	5	320	182	30.9	0.07	4.6E-09
G304C-1	10	310	68	30	0.10	1.7E-08
	10	320	33	31.1	0.08	2.9E-08
	10	290	34	31.4	0.08	2.9E-08
	10	270	29	31.6	<0.01	<5.0E-09
	10	280	51	31.6	0.04	1.0E-08
	10	300	64	31.6	<0.01	<5.0E-09
G304-10-1	10	340	76	30	<0.01	<5.0E-09
G304C-2	10	290	72	20.1	<0.01	<5.0E-09
	10	290	58	25.1	0.07	1.4E-08
	10	290	58	30.5	0.19	3.8E-08
G304D-1	15	320	33	31.5	0.22	7.7E-08
	15	290	34	32.1	0.08	2.9E-08
	15	270	29	32.2	<0.01	<5.0E-09
	15	280	51	32.5	0.01	<5.0E-09
	15	300	64	32.7	0.03	6.1E-09
	15	310	68	33	0.14	2.4E-08
G304D-2	15	290	72	15.3	<0.01	<5.0E-09
	15	290	58	19	0.09	1.8E-08
	15	290	58	23.1	0.30	6.0E-08
G304-15-2	15	340	76	34.2	0.60	9.2E-08
G304-15-TS-3	15	330	61	31.8	0.13	2.40E-08
G304-15-1	15	250	409	30.1	0.10	2.8E-09

Table 8
SCC growth rates of 304SS (20%CW, *T–S*).

Specimen no.	Cold work (%)	Temperature (°C)	Test time (days)	Apparent stress intensity factor (MPa$\sqrt{m}$)	Average crack length increment (mm)	Average crack growth rate (mm/s)
304E-3	20	290	35	27.8	0.13	4.3E-08
	20	290	50	13.8	0.08	1.8E-08
	20	290	63	18.5	0.13	2.4E-08
	20	290	48	22.9	0.13	3.1E-08
	20	290	50	23.6	0.17	4.1E-08
	20	290	21	18.8	0.05	2.7E-08
G304E-1	20	320	33	30.5	0.25	8.7E-08
	20	290	34	31	0.06	1.9E-08
	20	280	51	31.1	0.02	5.1E-09
	20	280	64	31.2	0.04	6.5E-09
	20	300	32	31.3	0.01	<5.0E-09
	20	310	19	31.4	0.05	2.9E-08
	20	310	17	31.6	0.05	3.3E-08
G304E-5	20	290	84	14	0.01	<5.0E-09
	20	320	27	9.17	<0.01	<5.0E-09
	20	320	84	14	0.03	3.7E-09
G304E-9	20	320	55	31.1	0.54	1.1E-07
	20	310	33	31.8	0.30	1.0E-07
	20	290	66	32.9	0.22	3.8E-08
	20	270	32	33.3	0.05	1.6E-08
	20	300	91	33.4	0.45	5.7E-08
G304-20-4	20	340	76	32.8	0.98	1.5E-07
G304 20-2	20	250	409	29.2	0.35	9.9E-09

the temperature was increased from 270 °C to 300 °C, the CGR of 304SS (20%CW) was increased, although retardation of the CGR ($<5 \times 10^{-9}$ mm/s) was observed in 316SS (20%CW)., According to Ozawa et al. [36], similar retardations of crack propagation in Alloy 600 have been confirmed by CGR measurements using CT specimens.

The fracture surface of the 316SS (20%CW), as shown in Fig. 8a, indicated that unfractured metallic segments remained in the SCC area. The existence of the metallic segments meant that the SCC susceptibility was not homogeneous. If the unfractured segments resisted the crack mouth opening, the crack growth could be arrested. From this consideration, it should be noted that even if the signal noise ratio is high enough and the test conditions are well controlled, reliability of CGRs in certain alloys is difficult to obtain. From this aspect, systematic investigations are required to elucidate the cracking phenomenon.

Figs. 8 and 9 show the fracture surfaces of 316SS (20%CW) and 304SS (20%CW) specimens; they exhibited similar surface morphologies. Typical IG facets were observed at the SCC area, and granular corrosion products, up to 2 μm in size, were scattered on the surfaces. Previously, it was reported that the corrosion products consisted of spinel type iron-rich oxide [15]. No obvious differences were observed between 316SS and 304SS.

In order to obtain systematic data, 83 crack growth tests were conducted using 38 specimens of 316SS with CW from 5% to 20%, as shown in Tables 3–5. The influences of CW, test temperature and applied stress on CGR were examined. Since the CGR of 316SS under simulated PWR conditions is slower than that under the oxygenated condition, average CGR measurement times of 53 days were needed to improve the data accuracy. In many cases a longer test time (maximum: 409 days) was used, while 22 tests were evaluated as below the detection limit or had no crack initiation. When the PDM is applied to monitor crack growth, theoretically the detection limit depends on the signal to noise ratio. However, CGR data for less than 10 μm crack length were regarded as being for an invalid length to eliminate the unknown error. It should be noted that several tests did not apply the PDM due to unavailability of the facility; in those cases, periodical loading was not performed as a starter for crack initiation. The purpose of periodical loading is to induce the transition from the transgranular (TG) fatigue precrack to the IG crack. This could affect reproducibility of SCC growth rates especially in low susceptibility specimens by reducing the effect of crack initiation period. The required crack length for less scatter of CGR measurements and the detection limit under high temperature conditions are discussed later.

In the same way, 49 CGRs of 304SS with 5–20%CW were measured using 16 specimens, and 12 CGRs were evaluated as below the measurable limit or no cracking was observed as listed in Tables 6–8. Since relatively low temperature tests were performed on 304SS, average test time for each CGR measurement was about 69 days. The total number of suitable CGRs was 98, excluding the 35 data omitted because they were below the detection limit.

4. Discussion

4.1. Influence of cold work

Fig. 10 illustrates the influence of CW on the CGR in 316SS specimens exposed to simulated PWR primary water conditions. Since it is difficult to measure the CW ratio of an actual component, Vickers hardness was used instead to describe the effect of CW. The acceleration effect on CGRs by CW clearly appeared for both 320 °C and 300 °C conditions. According to Tsubota et al. [37], the critical hardness for initiation of SCC for 316L stainless steel under simulated BWR conditions was HV = 300. On the other hand, the cracks propagated even for HV = 184 with 316SS (5%CW). This discrepancy indicates that the critical hardness for initiation is higher than that for propagation as CGR under BWR conditions is generally faster than that under PWR conditions.

A comparable enhancement effect on yield strength for 316L, 304, 304L and 347L stainless steels is well documented [8,12,13,29,38]. Comparing the absolute value of CGRs is difficult by reason of different test conditions and materials, but the tendency for an increase in CGR by cold working was consistent with the reported data as shown in Fig. 11.

In addition, the enhancement effect by high yield strength has been reported not only for stainless steel, but also nickel-based

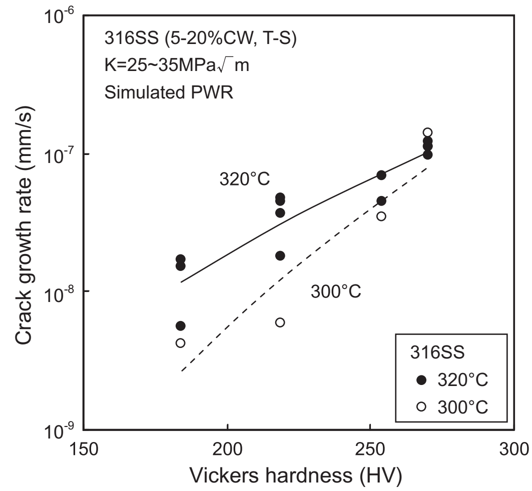

Fig. 10. Effect of hardness on crack growth rate of CW 316SS tested under simulated PWR primary water conditions. (Specimen Nos.: S6C5A, S6C10A, S6C10D, S6C10E, GS6C10-4, S6C15A, S6C15D, S6C15E, S6C20D, S6C2F, G316A8.)

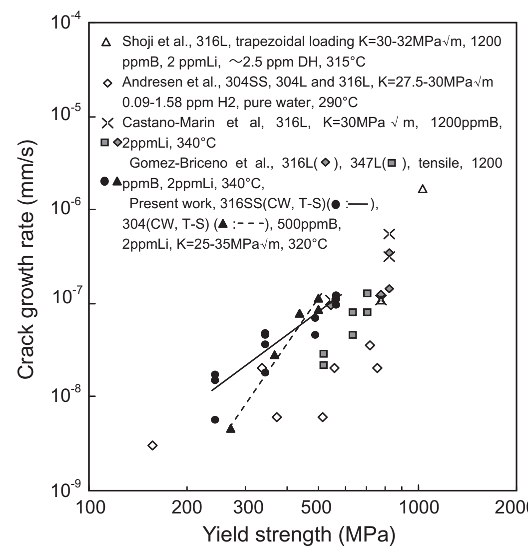

Fig. 11. Effect of yield strength on the crack growth rate of 316 and 316L under various simulated PWR primary water conditions [12,13,29,38]. (Specimen Nos.: S6C5A, S6C10A, S6C10E, GS6C10-4, S6C15A, S6C15E, S6C20D, S6C2F, G316A8, G304B-2, G304C-1, G304D-1, G304E-1, G304E-9.)

alloys which have been used as nuclear reactor component materials. Speidel and Magdowski [39] measured the CGRs of Alloy 600 by a double cantilever beam (DCB) test and found the CGRs could be expressed using the yield strength to the third power. Fig. 12 compares 316SS, 304SS and Alloy 600 as a function of yield strength. While the test methods were different, the figure indicated that similar yield strength dependency was observed between stainless steels and nickel-based alloy.

The corrosion phenomenon of these alloys does not correspond to the CGRs [40], therefore the effect of yield strength might not correlate to corrosion factors. The proposed role of high yield strength has been described by Andresen et al. [41] and Shoji et al. [12]: the plastic zone size at a crack tip becomes smaller in high yield strength alloys to provide a higher strain gradient.

The theoretical yield strength dependence is not clear, but empirically it can be described as the following equation (Fig. 12).

$$\mathrm{CGR} \propto \sigma_y^{\alpha} \; (\alpha = 2 - 3) \tag{1}$$

4.2. Influence of stress intensity factor

The crack growth rate is generally induced by the applied stress which the results from this study exhibit clearly as shown in Figs. 13 and 14. The apparent $K(K_a)$ dependence on CGR often is empirically described by the following relation:

$$\mathrm{CGR} \propto K_a^{\beta} \ (\beta = 0.6 - 3.2) \qquad (2)$$

where β is a constant that describes the K_a dependence. Fig. 13 shows the K_a dependence on 316SS indicated that 20%CW alloy provided a lower β value in comparison with 15%CW. However, it should be noted that this varying of trends was not obvious, if the data from $K_a = 13\ \mathrm{MPa}\sqrt{\mathrm{m}}$ were not there, there would be much slower CGRs with a fair amount of scatter due to difficulty of measurement. The CGRs of 316SS and 304SS obtained at 290 °C were slower and had more scatter as shown in Fig. 14. The statistical K_a dependence is discussed later, the obtained β for 316SS and 304SS ranged from 0.6 to 3.2.

The effect of K_a on CGRs has been evaluated for various alloys and water chemistry conditions as shown in Fig. 15. The acceleration effect by CW and temperature was recognized for several alloys, highest CGRs were observed for Alloy 600 with 31.9%CW in the *S*–*T* orientation. While CGRs were strongly influenced by the materials and test environment, comparable *K* dependences were observed in Alloy 600, 316SS and 304SS. This indicated that the influence of stress intensity on SCC was similar between nickel-based alloy and stainless steels under these conditions.

Regarding the threshold for the crack propagation, Scott [42] proposed that the threshold of Alloy 600 was $9\ \mathrm{MPa}\sqrt{\mathrm{m}}$ at 350 °C. The lowest K_a value of the present study was $13\ \mathrm{MPa}\sqrt{\mathrm{m}}$ for 316SS (15%CW). The existence of a threshold could not be elucidated because the data tended to be scattered for low CGR tests.

4.3. Influence of temperature on CGR

The temperature dependences of several cold-worked 316SS and 304SS specimens are shown in Figs. 16 and 17 respectively. The tests were performed under a constant load with an apparent stress intensity factor between 25 and 35 $\mathrm{MPa}\sqrt{\mathrm{m}}$. Arrhenius type temperature dependences were observed from 250 °C to 320 °C, but they disappeared above 330 °C in 15%CW and 10%CW 316SS specimens.

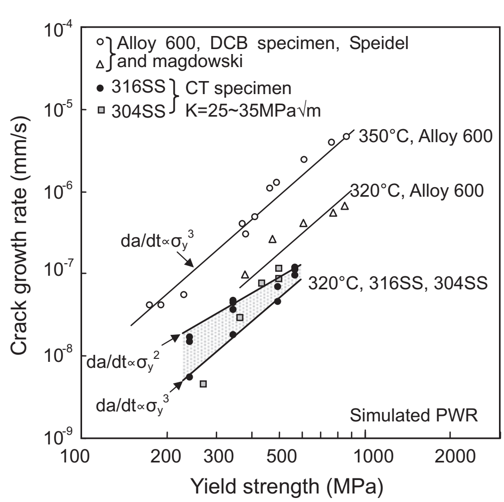

Fig. 12. Effect of yield strength on the crack growth rates of 316SS, 304SS and Alloy 600 [39]. (Specimen Nos.: S6C5A, S6C10A, S6C10E, GS6C10-4, S6C15A, S6C15E, S6C20D, S6C2F, G316A8, G304B-2, G304C-1, G304D-1, G304E-1, G304E-9.)

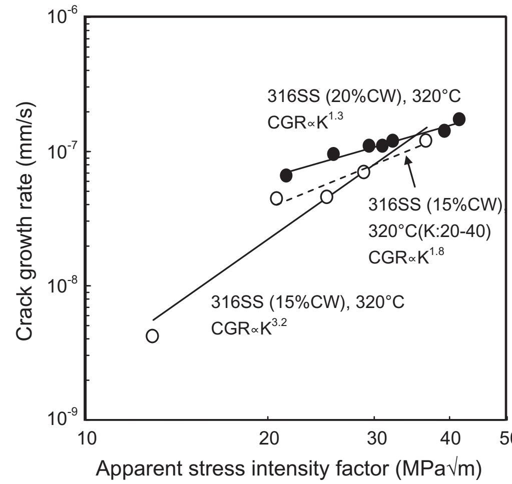

Fig. 13. Effect of stress intensity factor on the crack growth rates of 316SS with 20%CW and 15%CW at 320 °C. (Specimen Nos.: S6C20D, S6C2E, S6C2F, G316A8, S6C20-1, S6C15A, S6C15E, S6C15-4.)

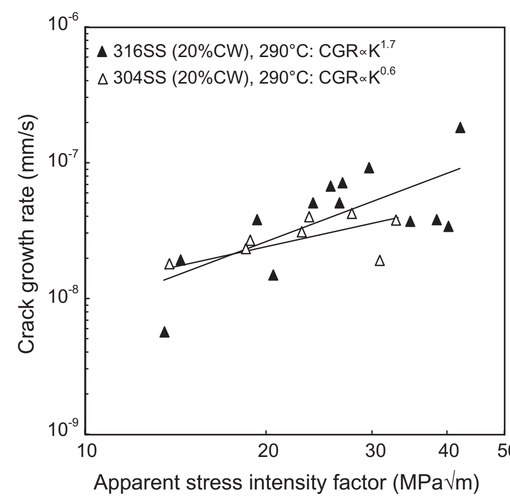

Fig. 14. Effect of stress intensity factor on the crack growth rates of 316SS (20%CW) and 304SS (20%CW) at 290 °C. (Specimen Nos.: S6C20D, S6C2E, G316A8, S6C20-1, S6C20-2, 304E-3, G304E-9.)

Because the PDM could not be applied above 330 °C, true CGRs in high temperature were not elucidated, but the results implied that the CGRs were inhibited at higher temperature particular in lower percent CW alloys. One of the explanations for the suppression effect is decreasing the corrosion rates of stainless steels in simulated PWR primary water conditions [43]. The reason for the suppression effect above 330 °C was not clear, but a surface electro-chemical reaction seemed to be the rate limiting process for the corrosion of specimens and SCC.

The estimated apparent activation energies, which were obtained using the least squares method, were 75 kJ/mol, 81 kJ/mol and 145 kJ/mol in 316SS with 20%CW, 15%CW and 10%CW, respectively, as shown in Fig. 16. On the other hand, the respective apparent activation energies of 304SS (20%CW) and 304SS (15%CW) were calculated as 91 kJ/mol and 90 kJ/mol. Estimated apparent activation energies always include CGR measurement errors, but the trend of apparent activation energy decreases with increasing percent of CW has been reported by Rebak et al. [19], Moshier and Brown [20], and Cassagne and Gelpi [44] in Alloy 600. In addition, according to Shoji et al. [12], no consistent effect of temperature on crack growth rate was obtained for higher percent CW 304L

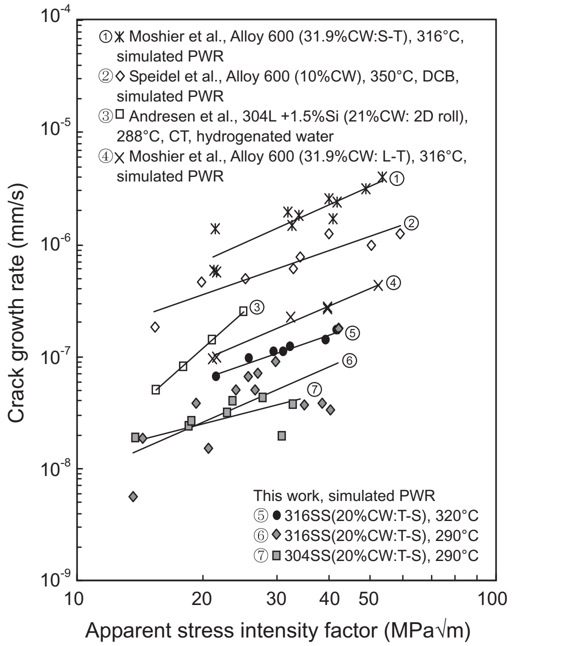

Fig. 15. Effect of stress intensity factor on CGR of various alloys in high temperature water [20,38,39]. (Specimen Nos.: S6C20D, S6C2E, S6C2F, G316A8, S6C20-1, S6C20-2, 304E-3, G304E-9.)

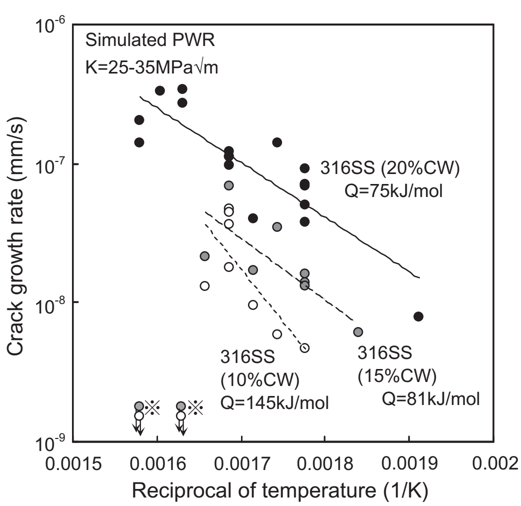

Fig. 16. Temperature dependence on crack growth rate of cold worked 316SS under simulated PWR primary water conditions. (Specimen Nos.: S6C20D, S6C2F, G316A8, S6C20-2, GCS6C20-K, GCS6C20-L, GCS6C20-M, GCS6C20-N, GCS6C20-O, G316 20 TS1, S6C15B, S6C15D, S6C15E, G316-15-TS-1, G316-15-TS-2, G316-15-TS-5, S6C10A, S6C10B, S6C10D, S6C10E, GS6C10-4, G316-10-TS-2, G316-10-TS-3.) ※ Data from total crack length less than 0.01 mm.

and 316L, which had yield strength of 750–1000 MPa. On the contrary, Speidel and Magdowski [39] reported no significant influence of CW on the temperature dependence in experiments using double cantilever beam specimens. All these data implied that mechanical properties have some potential to change the activation energy but it is difficult to determine the accurate activation energy.

Fig. 18 shows the temperature dependence on CGRs of cold worked stainless steels and Alloy 600 as reported from several sources [17,29,30,38,45,46]. Reported apparent activation energies in CW stainless steels were around 60 kJ/mol, while slightly higher values ranging from 75 to 145 kJ/mol were obtained in this study.

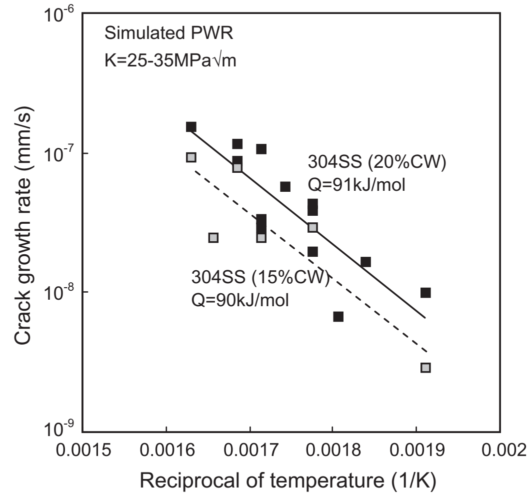

Fig. 17. Temperature dependence on crack growth rate of cold worked 304SS under simulated PWR primary water conditions. (Specimen Nos.: G304D-1, G304-15-2, G304-15-TS-3, G304-15-1, 304E-3, G304E-1, G304E-9, G304-20-4, G304-20-2.)

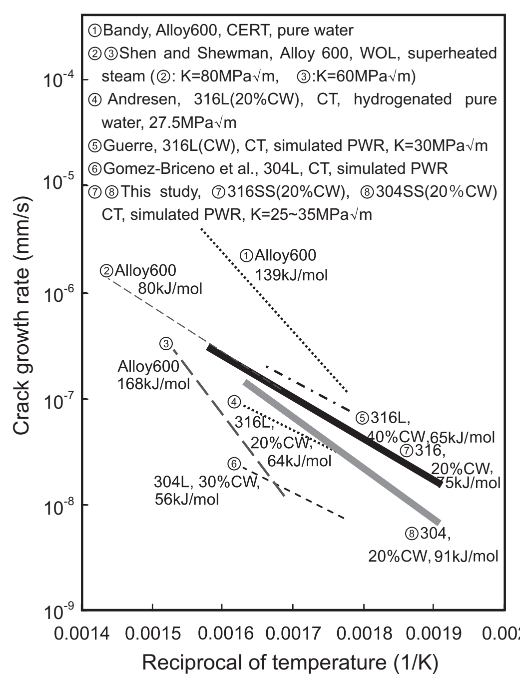

Fig. 18. Temperature dependence on crack growth rate of cold worked stainless steels and Alloy 600 under simulated PWR primary water and deaerated water conditions [17,29,30,38,45,46].

On the other hand, slightly higher apparent activation energies were reported for Alloy 600 ranging from 80 to 168 kJ/mol.

Arioka et al. [25] reported a similar temperature dependence for CGR in IG creep CGRs of 316SS. The CGRs of SCC were over 10 times higher, and a comparable thermal activation process might influence the crack growth.

4.4. Empirical formula for CGR calculation

This paper presents the influences of CW, stress intensity factor and temperature on the CGR of 316SS and 304SS. Each of the factors was precisely assumed as described above, but variability of data complicates the accurate prediction of CGRs. For instance the coefficient for yield strength (α) varies from 2 to 3 (Eq. (1)), the coefficient for apparent $K(\beta)$ ranges from 0.6 to 3.2 (Eq. (2)) and activation energy varies from 75 to 145 kJ/mol. If the mechanism is fully understood and accuracy of CGR measurement is enough, it might be possible to use each obtained parameter. However, CGRs of CW stainless steels under PWR conditions tend to be scattered and the role of each parameter has not been clarified, then statistical data treatment presents a feasible way to evaluate the CGRs.

In the study, the empirical formula was established from the obtained correlations as described in Eq. (3). Factors for yield strength, apparent stress intensity factor and temperatures were calculated by multivariable analysis using all CGRs obtained in the study except for those evaluated for a crack length less than 0.01 mm:

$$\frac{da}{dt} = 9.5 \times 10^{-10} \times \sigma_y^{2.9} \times K_a^{1.0} \times \exp^{\frac{-84\times10^3}{RT}} \tag{3}$$

where da/dt is crack growth rate (mm/s), σ_y is yield strength at test temperature, K_a is apparent stress intensity factor, R is gas constant (8.314 kJ/mol K) and T is absolute test temperature. SCC test results indicated the existence of a peak temperature, and the applicability range of the formula was between 250 °C and 320 °C. It should be noted that the base CGRs were for *T–S* orientation and cracking was branched, so technically, an absolute value for precise CGRs in operating power plants is not predictable.

Fig. 19 compares the calculated CGRs, which were derived from the empirical formula, and the measured CGRs; the data seemed to scatter in some extent. There are many reasons for variability of each measurement, for example crack arrest by an uncracked segment or specific material structures, and actual CGRs have some irregularities. In addition, PDM measurements of such low CGRs have some errors from electric noise, insulation of wires, etc. The empirical formula of Fig. 19 includes these irregularities and measurement errors from 98 CGRs. Theoretically, each factor might influence it mutually, then establishing the precise equation requires further fundamental studies.

Even though the precise CGR is not predictable, similar parameter dependences were observed between 316SS and 304SS. Both steel types were used with the same empirical formula and no obvious differences were observed. The results indicated that CGRs of 316SS and 304SS could be estimated using the same empirical formula.

Regarding the maintenance of operating power plants, the accuracy and margin of the safety ratio is important. Fig. 20 shows the frequency of distribution of measured/calculated CGR ratio; 92.8% of the measured CGRs did not exceed twice the calculated CGRs.

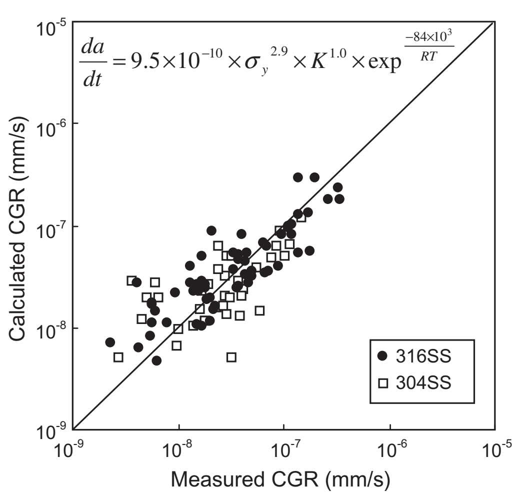

Fig. 19. Comparison of CGRs measured and calculated by the empirical formula.

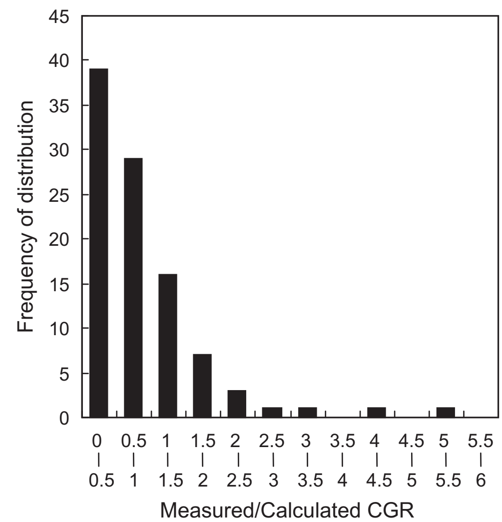

Fig. 20. Frequency of distribution as a function of measured/calculated CGR ratio.

5. Conclusions

The crack growth rates of 316SS and 304SS under simulated PWR primary water conditions have been summarized to develop an empirical formula providing better engineering applications. Fifty-three cold worked compact tension specimens were employed to clarify the influences of yield strength, temperature dependence and stress intensity factors:

(i) The influences of each parameter for 316SS and 304SS were similar, so the same empirical formula for crack growth rates could be applied. The estimated apparent activation energy was 84 kJ/mol and it was calculated from all the obtained crack growth rates. On the other hand, crack retardation was clearly observed above 330 °C in lower cold worked stainless steel specimens, therefore the applicability range of calculated activation energy was regarded as between 250 °C and 320 °C.
(ii) The crack growth rates increased with increasing yield strength for 5% and 20% cold worked 316SS and 304SS specimens. These rates were proportional to the 2.9 power of yield strength at test temperature.
(iii) The crack growth rates increased with increasing apparent stress intensity in the region between 13 MPa$\sqrt{m}$ and 40 MPa$\sqrt{m}$, and these rates were proportional to the apparent yield strength.
(iv) Cracking of *T–S* orientation specimens propagated through the grain boundary, and then branched off in two directions.

References

[1] W. Bamford, J. Hall, A review of alloy 600 cracking on operating nuclear plants including alloy 82 and 182 weld behavior, in: Proc. of ICONE12, ASME, 2004.
[2] D.W. Alley, A regulatory analysis and perspective regarding degradation of materials in light water reactors, in: Proc. of Corrosion 2011, Paper no. 11198, NACE, 2011.
[3] G.S. Was, P.L. Andresen, Corrosion 63 (1) (2007) 19.
[4] J.M. Boursier, S. Gallet, Y. Rouillon, et al., Stress corrosion cracking of austenitic stainless steels in PWR primary water: an update of metallurgical investigations performed on France withdrawn components, in: Proc. Int. Symp. Fontevraud 5, September 23–27, 2002.

[5] T. Couvant, P. Moulart, L. Legras, et al., PWSCC of austenitic stainless steels of heaters of pressurizers, in: Proc. Int. Symp Fontevraud, 6, 2006.
[6] Nuclear Industry Safety Agency (NISA), Cracks on the Inner Surface of the Welds at Primary Water Inlet and Outlet Nozzle to Steam Generators, NISA, February 5, 2008.
[7] N. Totsuka, Z. Szklarska-Smialowska, Corrosion 44 (1988) 124.
[8] P.L. Andresen, T.M. Angeliu, W.R. Catlin, et al., Effect of deformation on SCC of unsensitized stainless steel, in: Proc. of Corrosion 2000, Paper no. 203, NACE, 2000.
[9] P.L. Andresen, L.M. Young, W.R. Catlin, et al., Stress corrosion crack growth rate behavior of various grades of cold-worked stainless steel in high temperature water, in: Proc. of Corrosion 2002, Paper no. 2511, NACE, 2002.
[10] K. Arioka, Effect of temperature, hydrogen and boric acid concentration on IGSCC susceptibility of annealed 316 stainless steel, in: Proc. Int. Symp. Fontevraud 5, September 23–27, 2002.
[11] K. Arioka, T. Yamada, T. Takumi, Influence of boric acid, hydrogen concentration and grain boundary carbide on IGSCC behaviors of SUS 316 under PWR primary water, in: Proc. 11th Int. Conf. Environmental Degradation of Materials in Nuclear Power Systems-Water Reactors, Stevenson, August 10–14, 2003.
[12] T. Shoji, G. Li, J. Kwon, S. Matsushima, et al., Quantification of yield strength effects on IGSCC of austenitic stainless steels in high temperature water, in: Proc. 11th Int. Conf. Environmental Degradation of Materials in Nuclear Power Systems-Water Reactors, Stevenson, August 10–14, 2003.
[13] M.L. Castano Marin, M.S. Garcia Redondo, G.D. Velasco, et al., Crack growth rate of hardened austenitic stainless steels in BWR and PWR environments, in: Proc. 11th Int. Conf. Environmental Degradation of Materials in Nuclear Power Systems-Water Reactors, Stevenson, August 10–14, 2003.
[14] F. Vaillant, T. Couvant, J.M. Boursier, et al., Stress corrosion cracking of cold-worked austenitic stainless steels in laboratory primary PWR environment, in: Proc. PVP2004, San Diego, CA, July 25–29, 2004.
[15] T. Terachi, K. Fujii, K. Arioka, J. Nucl. Sci. Technol. 42 (2) (2005) 225.
[16] T. Couvant, L. Legras, F. Vaillant, Effect of strain-hardening on stress corrosion cracking of AISI 304L stainless steel in PWR primary environment at 360 ℃, in: Proc. 12th Int. Conf. Environmental Degradation of Materials in Nuclear Power Systems-Water Reactors, Salt Lake City, UT, August 14–18, 2005.
[17] C. Guerre, O. Raquet, E. Herms, et al., SCC growth behavior of austenitic stainless steels in PWR primary water conditions, in: Proc. 12th Int. Conf. Environmental Degradation of Materials in Nuclear Power Systems-Water Reactors, Salt Lake City, UT, August 14–18, 2005.
[18] K. Arioka, T. Yamada, T. Terachi, R.W. Staehle, Corrosion 62 (1) (2006) 74.
[19] R.B. Rebak, Z. Xia, Z.S. Smialowska, Corrosion 51 (9) (1995) 689.
[20] W.C. Moshier, C.M. Brown, Corrosion 56 (3) (2000) 307–320.
[21] Y.C. Gao, K.C. Hwang, Elastic–plastic fields in steady crack growth in a strain-hardening material, in: Proc. 5 th Int. Conf. on Fracture, Cannes, France, vol. 2, (1981) p. 669.
[22] L.M. Young, P.L. Andresen, T.M. Angeliu, Crack tip strain rate: estimates based on continuum theory and experimental measurement, in: Proc. of Corrosion 2001, Paper no.1131, NACE, 2001.
[23] T. Shoji, T. Yamamoto, K. Watanabe, et al., "3 DFEM simulation of EAC crack growth based on the deformation/oxidation mechanism, in: Proc. 11th Int. Conf. Environmental Degradation of Materials in Nuclear Power Systems-Water Reactors, Stevenson, August 10–14, 2003.
[24] P.L. Andresen, M.M. Morra, W.R. Catlin, Effect of yield strength, corrosion potential, composition and stress intensity factor in SCC of stainless steels, in: Proc. of Corrosion 2004, Paper no. 4678, NACE, 2004.
[25] K. Arioka, T. Yamada, T. Terachi, et al., Corrosion 63 (12) (2007) 1114.
[26] S. Lozano-Perez, T. Yamada, T. Terachi, et al., Acta Mater. 57 (18) (2009) 5361.
[27] K. Arioka, T. Yamada, T. Terachi, et al., Corrosion 62 (7) (2006) 568.
[28] D.J. Gooch, Mater. Sci. Eng. 91 (1987) 45.
[29] D. Gomez-Briceno, M. Sol Garcia, J. Lapena, SCC behavior of austenitic stainless steels in high temperature water effect of cold work, water chemistry and type of materials, in: Proc. 14th Int. Conf. Environmental Degradation of Materials in Nuclear Power Systems-Water Reactors, Virginia Beach, VA, August 23–27, 2009.
[30] C. Guerre, O. Raquet, E. Herms, et al., SCC crack growth rate of cold-worked austenitic stainless steels in pwr primary water conditions, in: Proc. 13th Int. Conf. Environmental Degradation of Materials in Nuclear Power Systems-Water Reactors, Whistler, Canada, August 19–23, 2007.
[31] Z. Lu, Y. Takeda, T. Shoji, J. Nucl. Mater. 383 (2008) 92.
[32] Japan Stainless Steel Association, Stainless Steels Handbook, Nikkan Kogyo Shimbun, Ltd., Japan, 384, 1995 (in Japanese).
[33] ASTM E 647-11. Standard Test Method for Measurement of Fatigue Crack Growth Rates. American Society for Testing and Materials, 2009.
[34] E. Richey, D.S. Morton, Influence of specimen size on the SCC growth rate of Ni-alloys exposed to high temperature water, in: Proc. of Corrosion 2006, Paper no. 6513, NACE, 2006.
[35] ASTM E 399-09. Standard Test Method for Plane-strain Fracture Toughness of Metallic Materials. American Society for Testing and Materials, 2011.
[36] M. Ozawa, Y. Yamamoto, K. Nakata, et al., Establishment of experimental conditions for the SCC growth rate test of alloy 600 and Ni base weld metal in high temperature oxygenated water, in: Proc. 12th Int. Conf. Environmental Degradation of Materials in Nuclear Power Systems-Water Reactors, Salt Lake City, UT, August 14–18, 2005.
[37] M. Tsubota, Y. Kanazawa, H. Inoue, The effect of cold work on the SCC susceptibility of austenitic stainless steels, in: Proc. 7th Int. Conf. Environmental Degradation of Materials in Nuclear Power Systems-Water Reactors, 1995, p. 519.
[38] P.L. Andresen, M.M. Morra, J. Nucl. Mater. 383 (2008) 97.
[39] M.O. Speidel, R. Magdowski, Stress corrosion cracking of stabilized austenitic stainless steels in various types of nuclear power plants, in: Proc. 9th Int. Conf. Environmental Degradation of Materials in Nuclear Power Systems-Water Reactors, Newport Beach, CA, August 1–5, 1999.
[40] T. Terachi, T. Yamada, K. Arioka, S. Lozano-Perez, Role of corrosion in LPSCC of Fe- and Ni- based alloys, in: Proc. of the Int. Symp. on Research for Light Water Reactors, 2007, p. 215.
[41] P.L. Andresen, L.M. Young, P.W. Emigh, R.M. Horn, Stress corrosion crack growth rate behavior of Ni alloys 182 and 600 in high temperature water, in: Proc. of Corrosion 2002, Paper no.2510, NACE, 2002.
[42] P. Scott, An analysis of primary water stress corrosion cracking in PWR steam generators, in: Proc. of the Specialists Meeting on Operating Experience with Steam Generators, Brussels, Belgium, 1991.
[43] T. Terachi, T. Miyamoto, T. Yamada, K. Arioka, Mechanistic study of LPSCC of stainless steels. Temperature dependence of corrosion in hydrogenated water, in: Proc. of Nuclear Plant Chemistry Conf., Quebec City, Canada, October 3–7, 2010.
[44] T. Cassagne, A. Gelpi, Crack growth rate measurements on alloy 600 steam generator turning in primary and hydrogenated AVT water, in: Proc. 6th Int. Conf. Environmental Degradation of Materials in Nuclear Power Systems-Water Reactors, San Diego, CA, August 1–5, 1993.
[45] Y. Shen, P.G. Shewmon, Corrosion 47 (9) (1991) 712.
[46] R. Bandy, D.C. Rooyen, Corrosion 40 (1984) 425.